Observational constraints on glyoxal production from isoprene oxidation and its contribution to organic aerosol over the Southeast United States

Jingyi Li[1], Jingqiu Mao[1,2], Kyung-Eun Min[3,4,*], Rebecca A. Washenfelder[3,4], Steven S. Brown[3,5], Jennifer Kaiser[6], Frank N. Keutsch[7], Rainer Volkamer[4,5], Glenn M. Wolfe[8,9], Thomas F. Hanisco[9], Ilana B. Pollack[10], Thomas B. Ryerson[3], Martin Graus[3,4,†], Jessica B. Gilman[3,4], Brian M. Lerner[3,4], Carsten Warneke[3,4], Joost A. de Gouw[3,4], Ann M. Middlebrook[3], Jin Liao[3,4], André Welti[3,4,‡], Barron H. Henderson[11], V. Faye McNeill[12], Samuel R. Hall[13], Kirk Ullmann[13], Leo J. Donner[2], Fabien Paulot[1,2], and Larry W. Horowitz[2]

[1]Program in Atmospheric and Oceanic Sciences, Princeton University, Princeton, New Jersey, USA
[2]Geophysical Fluid Dynamics Laboratory/National Oceanic and Atmospheric Administration, Princeton, New Jersey, USA
[3]Chemical Sciences Division, NOAA Earth System Research Laboratory, Boulder, Colorado, USA
[4]Cooperative Institute for Research in Environmental Sciences, University of Colorado Boulder, Boulder, Colorado, USA
[5]Department of Chemistry and Biochemistry, University of Colorado, Boulder, Colorado, USA
[6]Department of Chemistry, University of Wisconsin-Madison, Madison, Wisconsin, USA
[7]School of Engineering and Applied Sciences and Department of Chemistry and Chemical Biology, Harvard University, Cambridge, Massachusetts, USA
[8]Joint Center for Earth System Technology, University of Maryland Baltimore County, Baltimore, Maryland, USA
[9]Atmospheric Chemistry and Dynamics Lab, NASA Goddard Space Flight Center, Greenbelt, Maryland, USA
[10]Department of Atmospheric Science, Colorado State University, Fort Collins, Colorado, USA
[11]Department of Environmental Engineering Sciences, Engineering School of Sustainable Infrastructure and Environment, University of Florida, Gainesville, Florida, USA
[12]Department of Chemical Engineering, Columbia University, New York, New York, USA
[13]Atmospheric Chemistry Observation and Modeling Laboratory, National Center for Atmospheric Research, Boulder, Colorado, USA
[*]now at: School of Environmental Science and Engineering, Gwangju Institute of Science and Technology, Gwangju, South Korea
†now at: Institute of Meteorology and Geophysics, University of Innsbruck, Innsbruck, Austria
‡now at: Department of Experimental Aerosol and Cloud Microphysics, Leibniz Institute for Tropospheric Research (TROPOS), Leipzig, Germany

Corresponding author: Jingqiu Mao (Jingqiu.Mao@noaa.gov)

Key Points

- Box model simulated glyoxal production from three isoprene oxidation mechanisms differ greatly
- Aerosol uptake of glyoxal was constrained using airborne *in situ* measurements and a global model
- Model results show that glyoxal contributes 0-14% of SOA in the Southeast U.S. during summer

Abstract

We use a 0-D photochemical box model and a 3-D global chemistry-climate model, combined with observations from the NOAA Southeast Nexus (SENEX) aircraft campaign, to understand the sources and sinks of glyoxal over the Southeast United States. Box model simulations suggest a large difference in glyoxal production among three isoprene oxidation mechanisms (AM3ST, AM3B, and MCM v3.3.1). These mechanisms are then implemented into a 3-D global chemistry-climate model. Comparison with field observations shows that the average vertical profile of glyoxal is best reproduced by AM3ST with an effective reactive uptake coefficient γ_{glyx} of 2×10^{-3}, and AM3B without heterogeneous loss of glyoxal. The two mechanisms lead to 0-0.8 μg m^{-3} secondary organic aerosol (SOA) from glyoxal in the boundary layer of the Southeast U.S. in summer. We consider this to be the lower limit for the contribution of glyoxal to SOA, as other sources of glyoxal other than isoprene are not included in our model. In addition, we find that AM3B shows better agreement on both formaldehyde and the correlation between glyoxal and formaldehyde (R_{GF} = [GLYX]/[HCHO]), resulting from the suppression of δ-isoprene peroxy radicals (δ-$ISOPO_2$). We also find that MCM v3.3.1 may underestimate glyoxal production from isoprene oxidation, in part due to an underestimated yield from the reaction of IEPOX peroxy radicals (IEPOXOO) with HO_2. Our work highlights that the gas-phase production of glyoxal represents a large uncertainty in quantifying its contribution to SOA.

1 Introduction

Glyoxal (CHOCHO) is one of the most abundant dicarbonyl compounds in the atmosphere. Its sources include direct emissions from biofuel use and biomass burning,

and secondary production from oxidation of various volatile organic compounds (VOCs) [*Fu et al.*, 2008; *Hays et al.*, 2002; *Myriokefalitakis et al.*, 2008]. Glyoxal has a lifetime of about 1-3 hours against photolysis and oxidation by OH at midday [*Feierabend et al.*, 2009; *Volkamer et al.*, 2005; *Washenfelder et al.*, 2011]. It is highly water-soluble, with a Henry's Law constant of 3.0 - 4.2 $\times 10^5$ M atm^{-1} at 298 K [*Sander*, 2015]. In aerosol water, the solubility increases rapidly at low salt concentrations (up to 5.0 $\times 10^8$ M atm^{-1}) [*Kampf et al.*, 2013; *Waxman et al.*, 2015], due to the formation of glyoxal hydrate - sulfate complexes ("salting-in") [*Kurtén et al.*, 2015]. However, this increase is inhibited at high salt concentrations by the kinetic limitation of gas-particle partitioning [*Kampf et al.*, 2013; *Knote et al.*, 2014]. Laboratory and field studies showed that glyoxal readily undergoes heterogeneous uptake to aerosols and cloud droplets to form secondary organic aerosol (SOA) [*Carlton et al.*, 2007; *Ervens et al.*, 2011; *Galloway et al.*, 2009; *Galloway et al.*, 2011b; *Liggio et al.*, 2005a; b; *Lim et al.*, 2005; *Volkamer et al.*, 2007].

Glyoxal can provide important constraints on quantifying VOC emissions and oxidation mechanisms. Observations from aircraft, ground and satellite show that glyoxal is often highly correlated with formaldehyde (HCHO), another product of VOC oxidation [*DiGangi et al.*, 2012; *Kaiser et al.*, 2015; *MacDonald et al.*, 2012; *Miller et al.*, 2014; *Stavrakou et al.*, 2009; *Vrekoussis et al.*, 2010]. The ratio of glyoxal to formaldehyde (surface or tropospheric column concentrations), R_{GF}, varies for different biogenic and anthropogenic VOC precursors, so it can be used to quantify the source strength of local VOC emissions [*DiGangi et al.*, 2012; *Kaiser et al.*, 2015; *Miller et al.*, 2014; *Vrekoussis et al.*, 2010]. The NO_x (NO_x = NO + NO_2) dependence of R_{GF}, although it varies greatly for different VOCs and may offer additional information on VOC oxidation [*DiGangi et*

99 *al.*, 2012; *Kaiser et al.*, 2015; *Vrekoussis et al.*, 2010]. Thus, it is important to evaluate
100 model performance on R_{GF} and its NO_x dependence on regional and global scales,
101 providing critical information for present and future satellite validation [*Vrekoussis et al.*,
102 2010].

103 Sources and sinks of glyoxal remain largely uncertain [*Ervens et al.*, 2011; *Fu et al.*,
104 2008; *Galloway et al.*, 2011a; *Myriokefalitakis et al.*, 2008; *Stavrakou et al.*, 2009;
105 *Volkamer et al.*, 2007; *Washenfelder et al.*, 2011]. Production from isoprene oxidation
106 represents a major source of glyoxal on the global scale [*Fu et al.*, 2008]. Chamber
107 experiments suggest a significant yield (up to 3%) of glyoxal from the first generation of
108 isoprene oxidation under high NO_x conditions (500 ppbv NO) [*Galloway et al.*, 2011a;
109 *Volkamer et al.*, 2006]. As we show below, this high yield may not reflect the distribution
110 of β- and δ-isoprene peroxy radicals ($ISOPO_2$) as a function of their lifetimes under
111 ambient conditions [*Peeters et al.*, 2014]. Another large uncertainty lies in the
112 heterogeneous loss of glyoxal to aerosols and cloud droplets, which contributes to SOA
113 mass. Laboratory studies indicate that the uptake of glyoxal depends on aerosol and cloud
114 composition [*Corrigan et al.*, 2008; *Jang et al.*, 2002; *Kroll et al.*, 2005; *Liggio et al.*,
115 2005a; b; *Noziè re et al.*, 2009; *Volkamer et al.*, 2009; *Waxman et al.*, 2015], ambient
116 relative humidity (RH) [*Corrigan et al.*, 2008; *Hastings et al.*, 2005; *Kampf et al.*, 2013;
117 *Liggio et al.*, 2005a] and temperature [*Gomez et al.*, 2015]. By assuming irreversible
118 reactive uptake with an uptake coefficient $\gamma_{glyx} = 2.9 \times 10^{-3}$, *Fu et al.* [2008] found that
119 this process accounts for 14% of glyoxal loss globally. *Volkamer et al.* [2007] estimated
120 γ_{glyx} of 3.7×10^{-3} in Mexico City, where glyoxal contributes about 15% of ambient SOA.
121 A much lower γ_{glyx} (0-8×10^{-4} for the day and $(2 \pm 1) \times 10^{-4}$ for the night) was derived in

Los Angeles [*Washenfelder et al.*, 2011], where kinetic limitations at the high salt concentrations likely reduce the rate of SOA formation [*Kampf et al.*, 2013; *Knote et al.*, 2014].

The Southeast Nexus (SENEX) aircraft campaign, which took place in June–July of 2013, aimed to improve the understanding of the interactions between biogenic and anthropogenic emissions over the Southeast U.S. It provided a detailed characterization of tropospheric photochemistry (gas and aerosol), including ozone, NO_y (NO, NO_2 and its atmospheric oxidation products), biogenic VOCs (isoprene, terpene), isoprene oxidation products and organic aerosols [*Warneke et al.*, 2016]. In particular, glyoxal was measured on board the NOAA WP-3D aircraft using a cavity enhanced absorption spectroscopy technique [*Min et al.*, 2015], and formaldehyde was measured using laser induced fluorescence technique [*Cazorla et al.*, 2015]. These measurements provide an unprecedented opportunity to examine the sources and sinks of glyoxal in this region, as well as its contribution to SOA mass.

Here we first examine the glyoxal yield from isoprene oxidation in a box model with three chemical mechanisms (AM3ST, AM3B, and the Master Chemical Mechanism v3.3.1 [*Jenkin et al.*, 2015]). We then use field observations from the SENEX field campaign, interpreted with a chemistry-climate model, to understand the sources and sinks of glyoxal over the Southeast U.S. The comparison of the model to high resolution aircraft data for both glyoxal and formaldehyde provides important new constraints on the potential for glyoxal to form SOA, but also highlights uncertainty in the mechanism for isoprene oxidation, the single largest source of glyoxal in the Southeast U.S.

2 Methods

AM3 is the atmospheric component of the Geophysical Fluid Dynamics Laboratory (GFDL) coupled model CM3. The dynamical core, physical parameterizations, cloud and precipitation processes, and cloud-aerosol interactions in AM3 are described in detail in *Donner et al.* [2011]. Chemistry in a previous version of AM3 has been described by *Naik et al.* [2013]. In this work, we nudge the horizontal wind field in the model toward values from the NCEP Global Forecast System (GFS), allowing the model to simulate synoptic conditions corresponding to those sampled during field campaigns [*Lin et al.*, 2012]. We also apply finer vertical grids for convection plumes than the standard AM3 to improve the wet removal of tracers during summer time [*Paulot et al.*, 2015]. The photolysis module has been updated to Fast-JX v7.1 (ftp://128.200.14.8/public/prather/Fast-J), to compute the impacts from aerosols and clouds interactively. Dry deposition velocities prescribed in the model reflect rapid dry deposition of oxidized organic compounds [*Nguyen et al.*, 2015].

Biogenic emission of isoprene is computed using the Model of Emissions of Gases and Aerosols from Nature (MEGAN) inventory [*Guenther et al.*, 2006], with a total 15.9 Tg C in North America in June-August of 2013, which is slightly higher than previous estimates of 12.2-14.6 Tg C (June-August of 2006) in the same region [*Millet et al.*, 2008]. We reduce the isoprene emissions estimated by MEGAN by 20% (to 12.7 Tg C), to be consistent with other estimates of isoprene emission over the Southeast U.S. [*Warneke et al.*, 2010]. We do not consider glyoxal production from oxidation of terpenes and aromatics in this work, as their contribution is relatively small compared to isoprene over the Southeast U.S. [*Kaiser et al.*, 2015]. Inclusion of larger isoprene emissions and

other VOC sources would proportionally increase the magnitude of glyoxal sinks derived in the analysis below. Anthropogenic emissions in 2013 follow the Representative Concentration Pathway 8.5 (RCP 8.5) projection [*Lamarque et al.*, 2011]. We applied diurnal variation anthropogenic NO_x emissions in North America following *Mao et al.* [2013b]. Anthropogenic NO_x emissions in RCP 8.5 are 0.34 Tg N/month over North America, comparable to the estimate from NEI 2011 of 0.29 Tg N/month [*Travis et al.*, 2015]. We reduce these anthropogenic NO_x emissions by 25% to 0.26 Tg N/month, to be consistent with recent estimates in this region [*Anderson et al.*, 2014].

2.1 Isoprene chemistry

The standard isoprene mechanism used in AM3, "AM3ST", is largely based on *Mao et al.* [2013b] following chamber observations from *Paulot et al.* [2009a; 2009b] and *Crounse et al.* [2011]. The main features of this mechanism include: (1) substantial yield (7%) of first generation organic nitrates from δ-$ISOPO_2$, compared to 4.7% from β-$ISOPO_2$; (2) detailed assignment of the fate of first- and second-generation organic nitrates; and (3) isomerization of $ISOPO_2$ using the laboratory-determined rate constants. We further update this chemistry in several aspects. First, we assume a 25% molar yield of glyoxal from $ISOPO_2$ isomerization as the first-generation product [*Marais et al.*, 2016]. Second, the reaction of $ISOPO_2$ with HO_2 is updated following *St. Clair et al.* [2016a] to reflect a higher yield of unsaturated hydroxy hydroperoxides (ISOPOOH) (94%). Third, we adopt a new methylvinyl ketone (MVK) oxidation chemistry in which the glycolaldehyde molar yield is increased from 0.53 to 0.72 under high NO_x conditions [*Praske et al.*, 2015]. Fourth, we include fast photolysis of carbonyl organic nitrates [*Müller et al.*, 2014]. Fifth, we adopt a substantially slower ozonolysis rate of isoprene β-

hydroxy nitrate (ISOPNB, 3.7 $\times 10^{-19}$ molec^{-1}cm^{3}s^{-1} [*Lee et al.*, 2014]) than the previous value from *Lockwood et al.* [2010] (1.06 $\times 10^{-16}$ molec^{-1}cm^{3}s^{-1}). Lastly, we update the NO_3-initiated chemistry of isoprene following MCM v3.2 [*Jenkin et al.*, 1997; *Saunders et al.*, 2003]. As illustrated in Figure S1, glyoxal is produced in the first generation of isoprene oxidation, both from the decomposition of alkoxyl radical (DIBOO shown in Figure S1) through the δ-channel under high NO_x conditions [*Peeters and Nguyen*, 2012], and from isomerization of $ISOPO_2$ under low NO_x conditions [*Stavrakou et al.*, 2010]. Glyoxal is further produced in later generations from oxidation of carbonyl compounds including glycolaldehyde and isoprene epoxydiol (IEPOX).

In this work, we introduce an additional mechanism, "AM3_beta" (AM3B), to reflect more recent updates to the understanding of isoprene oxidation. Both theoretical and experimental studies indicate that β- and δ-$ISOPO_2$ undergo fast interconversion [*Bates et al.*, 2014; *Crounse et al.*, 2011; *Peeters et al.*, 2014]. One important implication is that oxidation products observed in experimental chambers at ~500 ppbv NO may not reflect the products in ambient air where NO is several orders of magnitude lower. This is due to a higher fraction of δ-$ISOPO_2$ loss via bimolecular reactions than interconversion back to β-$ISOPO_2$ under high NO_x conditions. To reflect this change, we only allow β-$ISOPO_2$ to react with NO because δ-$ISOPO_2$ is believed to only account for < 3% of total $ISOPO_2$ under ambient conditions [*Peeters et al.*, 2014]. The yield of β-hydroxyl isoprene nitrate (ISOPNB) is assumed to be 0.1, an average of the suggested values 0.09 [*Xiong et al.*, 2015] and 0.16 [*Teng et al.*, 2015]. The yields of HCHO, MVK and methacrolein (MACR) from β-$ISOPO_2$ + NO are adjusted accordingly for carbon balance. As we show

below, this update changes the production of formaldehyde and glyoxal under high NO_x conditions.

The Leeds Master Chemical Mechanism (MCM) is a near-explicit chemical mechanism that describes gas-phase VOC chemistry. The latest revision, v3.3.1, includes recent updates for OH-initiated isoprene chemistry [*Jenkin et al.*, 2015], such as isoprene-peroxy radical interconversion and isomerization pathways [*Peeters et al.*, 2014], and the chemistry of IEPOX [*Bates et al.*, 2014; *Paulot et al.*, 2009b]. Consequently, these updates show significant differences in simulated HO_x (HO_x = OH + HO_2), NO_x and major oxidation products compared to earlier versions of MCM. To evaluate the performance of MCM v3.3.1 in our global model, we implement a MCM-like mechanism ('AM3M') by adjusting the production of glyoxal from major pathways in the AM3B mechanism, to approximate the glyoxal and HCHO yields of MCM v3.3.1 in a highly condensed chemical mechanism suitable for use in a global model (Figure S2).

2.2 Heterogeneous loss of glyoxal and methylglyoxal

Heterogeneous loss onto aerosols and cloud droplets plays an important role in the fate of dicarbonyls. Here we assume this process is irreversible and can be represented by a first-order reactive uptake rate constant *k* [*Mao et al.*, 2010]

$$k = \left(\frac{a}{D_g} + \frac{4}{v\gamma}\right)^{-1} A$$

where a is the effective radius of aerosols or cloud droplets, D_g is the gas phase diffusion constant, γ is the reactive uptake coefficient, A is the surface area of aerosols or cloud droplets, and v is the mean molecular velocity of the gas molecule.

We allow this process to take place on five types of aerosols including sulfate, black carbon (BC), primary organic carbon (POC), sea salt, mineral dust and SOA, with hygroscopic growth included [*Mao et al.*, 2013a]. Given the large uncertainties associated with the uptake of glyoxal, we use field observations to assess the possible range of γ_{glyx}. We do not include glyoxal uptake by cloud droplets in this work, because the uptake coefficient by aerosols is much greater, and because large uncertainties are associated with mixing of cloudy and no-cloud volumes within a grid box [*Huijnen et al.*, 2014; *Jacob*, 2000]. We include heterogeneous loss of methylglyoxal with an uptake coefficient of 7.6×10^{-3} [*Zhao et al.*, 2006], to produce better closure with total organic aerosol (OA) in the model.

The irreversible surface uptake coefficient, γ_{glyx} applied here should be viewed as an "effective reactive uptake coefficient", to simply represent the net heterogeneous loss of glyoxal that does not revert back to the gas-phase, and provide an estimate for its contribution to SOA mass on the regional scale. Previous studies have indicated that this process is likely reversible to some extent [*Galloway et al.*, 2009; *Kroll et al.*, 2005]. We show below that the values of γ_{glyx} are dependent on the choice of gas-phase chemistry.

3 NO_x-Dependent Glyoxal and HCHO Yields

We first conduct box model simulations to quantify the yield of glyoxal and HCHO from isoprene oxidation as a function of NO_x levels, using the Dynamically Simple Model of Atmospheric Chemical Complexity (DSMACC) [*Emmerson and Evans*, 2009]. We test three mechanisms (AM3ST, AM3B, and MCM v3.3.1) in the model. The model is initialized at 8:00 local time (LT) for mid-latitude summer conditions, with 1 ppbv of

isoprene, 60 ppbv of ozone, 150 ppbv of CO, and a choice of 0.01, 0.1 or 1 ppbv of NO_x. While NO_x is held constant, isoprene is allowed to decay over time. Figure 1 shows the cumulative yields of glyoxal and HCHO per unit carbon from isoprene oxidation at various NO_x levels after three days of model integration with their loss processes turned off [*Palmer et al.*, 2003]. We also use tagged tracers for individual pathways (β/δ-$ISOPO_2$ + NO, $ISOPO_2$ + HO_2, isomerization of $ISOPO_2$) to compute their contribution in each mechanism.

A striking difference between the MCM v3.3.1 and AM3 mechanisms is the glyoxal production under low NO_x conditions. While the AM3 mechanisms show a large yield of glyoxal from isomerization of $ISOPO_2$ and the oxidation of IEPOX (via the $ISOPO_2$ + HO_2 pathway), MCM v3.3.1 shows very little production of glyoxal from these channels. For the isomerization pathway, MCM v3.3.1 assumes 50% of 1,6-H shift isomerization flux produces hydroperoxy-aldehydes (HPALDs), with another 50% produces complex dihydroperoxy formyl peroxy radicals, referred as "di-HPCARPs" by *Peeters et al.* [2014]. MCM v3.3.1 includes low production of glyoxal from the degradation of HPALDs and di-HPCARPs. On the other hand, the AM3 mechanisms do not include di-HPCARPs, and assume fast photolysis as the only loss process of HPALDs, with prompt yield of glyoxal following *Stavrakou et al.* [2010].

Another large difference in glyoxal yield comes from the treatment of the $ISOPO_2$ + HO_2 pathway, particularly regarding the fate of IEPOX. MCM v3.3.1 assumes a major production of organic peroxides from the reaction of IEPOX peroxy radicals (IEPOXOO) (α-carbonyl peroxy radicals) with HO_2, while AM3 mechanisms follow *Paulot et al.* [2009b] and assume full radical propagation for this reaction, with a 28% yield of glyoxal.

As a result, a much higher yield of glyoxal is predicted from the $ISOPO_2$ + HO_2 pathway in the AM3 mechanisms compared to MCM v3.3.1. In fact, several studies have confirmed significant OH production from the reaction of HO_2 with α-carbonyl peroxy radicals [*Dillon and Crowley*, 2008; *Hasson et al.*, 2004; *Jenkin et al.*, 2007]. This is also consistent with recent studies of IEPOX kinetics, which show very little formation of peroxides under low NO_x conditions [*Bates et al.*, 2014; *Jacobs et al.*, 2013].

Under high NO_x conditions, the three mechanisms show better agreement for glyoxal production, though with different pathways contributing. MCM v3.3.1 shows a dominant production from the β-$ISOPO_2$ + NO pathway, mainly due to a higher yield of glyoxal from oxidation of glycolaldehyde (20%), based on *Niki et al.* [1987]. An even higher yield of glyoxal (29%) was adopted by *Galloway et al.* [2011a]. In contrast, the AM3 mechanisms apply a lower yield of glyoxal (13%) following *Butkovskaya et al.* [2006]. Surprisingly, both AM3ST and AM3B show significant production from isomerization of $ISOPO_2$ and the $ISOPO_2$ + HO_2 pathway, suggesting the potential importance of these channels for glyoxal production even under high NO_x conditions. AM3ST has a major production from the δ-$ISOPO_2$ + NO pathway, leading to 60% higher glyoxal yield than AM3B. MCM v3.3.1 shows a small contribution from the δ-$ISOPO_2$ + NO channel, due to a small fraction of δ-$ISOPO_2$ in the radical pool of $ISOPO_2$ (< 3%). This reflects a different distribution of δ-$ISOPO_2$ and β-$ISOPO_2$ under ambient conditions vs. very high NO chamber conditions [*Peeters et al.*, 2014], consistent with our assumption in AM3B. Overall, the AM3 mechanisms show decreasing glyoxal production with increasing NO_x concentration, whereas MCM v3.3.1 shows the opposite.

The HCHO yield and its NO_x dependence appear to be more consistent across the different mechanisms. Under low NO_x conditions, isomerization of $ISOPO_2$ and the $ISOPO_2 + HO_2$ pathway contribute most to HCHO. At $NO_x = 1$ ppbv, the $ISOPO_2 + NO$ pathway becomes the primary source of HCHO. The HCHO yield in AM3B is 17% higher than AM3ST and comparable to MCM v3.3.1, mainly due to a higher HCHO yield from the β-$ISOPO_2 + NO$ pathway than the δ-$ISOPO_2 + NO$ pathway. It should be noted that the cumulative yields shown in Figure 1 represent the potential glyoxal and HCHO produced from sufficient oxidation of 1 ppbv isoprene and the intermediate VOCs. This is different from ambient conditions that isoprene is continuously emitted and the production of glyoxal and HCHO are dependent on OH levels (i.e. the production rate of $ISOPO_2$). Chemical loss of HCHO and glyoxal are similar across the mechanisms (Table S1).

The NO_x dependent yields of glyoxal and HCHO from box model results are useful to identify their major production pathways at different NO_x levels. This knowledge can be translated to 3D model outputs and help evaluate model performance from these pathways using aircraft observations.

4 Observational Constrains on Glyoxal Production

4.1 Vertical profiles of gaseous and particulate species

We compare the AM3 model predictions for glyoxal, formaldehyde, and isoprene oxidation products to measurements of these species acquired during the SENEX field campaign. All measurements are averaged to 1 minute time resolution. The measurement accuracies for isoprene, formaldehyde, NO_x, glyoxal, organic aerosol and aerosol surface

area are 25%, 10%, 5%, 5.8%, 50%, and 36% respectively ([*Warneke et al.*, 2016] and the references therein). Although other carbonyl compounds have recently been found to suffer from inlet artifacts arising from catalytic conversion of organic hydroperoxides on metal inlet surfaces [*Rivera-Rios et al.*, 2014], we do not expect such interferences for glyoxal since no metal surfaces are present in the glyoxal sampling line [*Min et al.*, 2015], and since there are currently no known mechanisms for conversion of hydroperoxides to glyoxal. We also expect little interferences for formaldehyde since its residence time during exposure to metal surfaces is very small [*Cazorla et al.*, 2015], This is confirmed by recent laboratory tests, suggesting the interference is < 5% for this specific instrument [*St. Clair et al.*, 2016b]. We exclude biomass burning, urban plumes, stratospheric air ($CH_3CN \geq 225$ pptv, $NO_x/NO_y > 0.4$ or $NO_2 > 4$ ppbv or $O_3/CO > 1.25$ mol/mol, respectively) from our analysis following *Hudman et al.* [2007], and omit data from the Ozark Mountains, where the model shows a significant positive bias for isoprene (Figure S3). We also exclude nighttime flights from our analysis.

Figure 2 shows the mean vertical profiles of observed and modeled isoprene, glyoxal, HCHO and other related species during SENEX. Model output is sampled along the flight tracks and at the flight time with 1 hour time resolution. We include two model simulations (AM3ST and AM3B). MCM v3.3.1 is not included because of its complexity. Instead, we show AM3M in our global model as a proxy to MCM v3.3.1 in the following sections. Simulated NO_x agrees with the observations at all altitudes except for a slight overestimate (~20%) near the surface. Observed isoprene concentration peaks near the surface at 1.2 ppbv and decreases gradually with altitude. Both AM3ST and AM3B show a positive bias of isoprene below 1 km, but no such bias is evident for HCHO. As HCHO

in this region is dominantly produced from isoprene and has a relatively longer lifetime than that of isoprene (4 h vs. < 1 h), we attribute this positive bias of modeled isoprene partly to sampling bias and partly to shallow boundary layer and slow vertical mixing in the current model. We further examine modeled OH and J values using ICARTT (2004) [*Mao et al.*, 2013b] and NOMADSS (2013) (https://www.eol.ucar.edu/field_projects/nomadss) field observations over the eastern U.S., and we find that the model agrees with observed OH and J values within 20% (Figure S4 and S5).

Like isoprene, both HCHO and glyoxal decrease with altitude, reflecting their short photochemical lifetimes (4 h and 3.5 h) and their dominant source from isoprene. Our model is able to reproduce their vertical gradients, although the vertical profiles of HCHO and glyoxal appear to be sensitive to the choice of photochemical mechanisms. AM3ST underestimates HCHO by 32% and overestimates glyoxal almost by a factor of two near the surface. With the suppression of δ-$ISOPO_2$ in AM3B, HCHO is increased by 17% and glyoxal is decreased by 38% near the surface, leading to better agreement with observations for both species.

The abundance of glyoxal is also dependent on its heterogeneous loss. By assuming an irreversible reactive uptake on aerosols, an optimal value of γ_{glyx} is selected to minimize the difference between modeled and observed glyoxal in the boundary layer. We find that the best agreement is achieved for AM3ST with γ_{glyx} of 2×10^{-3} and for AM3B with γ_{glyx} of zero (Table S2); we adopt those values in the following analysis.

γ_{glyx} derived with AM3B is lower than the value from previous laboratory experiments (2.9×10^{-3} by *Liggio et al*. [2005b]), likely due to two reasons. First, there could be a missing source of gas-phase glyoxal in the current mechanism, which can be compensated by aerosol uptake and lead to a higher contribution to SOA formation. We find that approximate 30% increase of glyoxal production in AM3B would be required to compensate aerosol uptake of glyoxal with $\gamma_{glyx} = 2.9 \times 10^{-3}$. Second, the effective aerosol uptake coefficient, as we assumed here to represent the net heterogeneous loss of glyoxal, is indeed smaller than the value from the previous study. One possibility is that the aerosol uptake of glyoxal is to some extent reversible [*Galloway et al.*, 2009; *Kroll et al.*, 2005], which would lead to a lower estimate of γ_{glyx}. Another possibility is the suppression of glyoxal loss to ambient aerosols that are internally mixed with organic and inorganic components, resulting from its organic coating [*Galloway et al.*, 2011b]. It is also possible that additional production of glyoxal in the particle-phase from other organic compounds reduces the net loss of glyoxal to the aerosol surface. In fact, the negligibly small uptake coefficients of glyoxal ($0\text{-}8 \times 10^{-4}$ during the daytime and $(2 \pm 1) \times 10^{-4}$ during the nighttime) have also been determined from analysis of glyoxal observations in a previous field study in Los Angeles during the CalNex field campaign [*Washenfelder et al.*, 2011].

Overall, the resulting average contribution of glyoxal to organic aerosols is about 0.8 $\mu g\ m^{-3}$ for AM3ST (Figure S7) and negligible for AM3B in the boundary layer over the Southeast U.S. We emphasize that this is likely the lower limit of glyoxal SOA, as other glyoxal sources such as anthropogenic VOCs and monoterpenes, are not included in our model. Accounting for these additional sources would require a higher sink of glyoxal,

and therefore results in higher glyoxal SOA. The estimate from AM3ST is comparable to previous model studies over the same region assuming reversible or irreversible reactive uptake of glyoxal onto aerosols [*Knote et al.*, 2014; *Li et al.*, 2015; *Ying et al.*, 2015], while AM3B is not. We also find that the inclusion of IEPOX aerosol uptake may reduce glyoxal in the boundary layer by less than 15% over the Southeast U.S. (Figure S8). This would lead to an even lower estimate of glyoxal SOA.

4.2 R_{GF} and its dependence on NO_x

Comparison of modeled and observed R_{GF} provides additional constraint on the gas-phase chemistry for glyoxal production. Figure 3 shows the co-variation of glyoxal and formaldehyde in the boundary layer during SENEX. The linear regression slope (R_{GF}) derived from observations is 2.4% (R^2=0.61) in the boundary layer over the Southeast US, suggesting that the dominant source of both glyoxal and formaldehyde in this region is isoprene [*Kaiser et al.*, 2015]. The AM3ST mechanism overestimates R_{GF} by a factor of two, while better agreement is achieved by the AM3B mechanism, due to the suppressed production of glyoxal and enhanced production of HCHO. Simulations with both mechanisms significantly underestimate the range of HCHO concentrations observed. Without heterogeneous loss of glyoxal, the model with AM3ST significantly overestimates R_{GF} but predicts a similar result as assuming no heterogeneous loss of glyoxal with AM3B.

We further examine the NO_x dependence of HCHO, glyoxal and R_{GF} during SENEX (Figure 4). A prominent feature of Figure 4 is the high similarity between the observed NO_x-dependence of HCHO and glyoxal. Both HCHO and glyoxal are observed to

increase with NO_x concentrations and to start to level off at 1 ppbv of NO_x. Remarkably, R_{GF} shows little variation across NO_x concentrations, consistent with *Kaiser et al.* [2015]. Both AM3ST and AM3B are able to reproduce the NO_x dependence of HCHO, although they tend to underestimate HCHO by 1-2 ppbv across NO_x regimes, consistent with *Wolfe et al.* [2016]. AM3B shows better agreement with observations than AM3ST at high NO_x level, indicating δ-channel is suppressed under ambient conditions. Using the optimized γ_{glyx} values described above (2×10^{-3} for AM3ST and zero for AM3B), our model can roughly capture the NO_x dependence of glyoxal. In contrast to Figure 1, neither AM3ST nor AM3B shows high glyoxal concentrations under low NO_x conditions, reflecting slower production of glyoxal under such conditions due to low OH radical concentrations and slow $ISOPO_2$ production rate in the ambient atmosphere [*Wolfe et al.*, 2016]. Although the NO_x dependent HCHO and glyoxal are individually captured qualitatively, a large positive bias in R_{GF} is apparent for AM3ST across NO_x regimes and for AM3B at $NO_x < 0.5$ ppbv. We attribute the bias in AM3ST to the overestimate of glyoxal under low NO_x and underestimate of HCHO across NO_x regimes. The bias in AM3B is mainly due to the underestimate of HCHO.

To examine the NO_x dependence of HCHO, glyoxal and R_{GF} from MCM v3.3.1, the AM3M mechanism that mimics MCM v3.3.1 is then tested in our AM3 global model. Comparison to the SENEX data (Figure 4) shows that AM3M can also well reproduce the NO_x dependence of HCHO, similar to the performance of other AM3 mechanisms. However, AM3M largely underestimates glyoxal and R_{GF} across all NO_x levels, suggesting additional sources of glyoxal needed in the current MCM mechanism. Inclusion of heterogeneous loss of glyoxal would further reduce glyoxal in AM3M and

433 worsen the comparison. One possible reason for the underestimate of glyoxal in AM3M
434 is the lack of a radical propagating channel for the IEPOXOO + HO_2 reaction in MCM
435 v3.3.1, as described above.

436 R_{GF} provides a useful tool to estimate global production of glyoxal from isoprene
437 oxidation. In particular, the fact that R_{GF} is insensitive to NO_x allows us to directly
438 compute its global production rate. Assuming 0.4 HCHO yield per isoprene C (Figure 1,
439 also consistent with *Palmer et al.* [2003]) and a global constant R_{GF} of 2.4% (according to
440 the measurements during SENEX), we can derive the global production of 23 Tg glyoxal
441 with 500 Tg isoprene emitted annually [*Guenther et al.*, 2006]. This is similar to a
442 previous estimate of 21 Tg yr^{-1} glyoxal from isoprene [*Fu et al.*, 2008].

443 **5 Budget of Glyoxal in North America**

444 Table 1 summarizes the monthly averaged glyoxal budget over North America
445 (20 ~55 °N, 60 ~130 °W) in the boundary layer (0-1.5 km) during June-July of 2013 for
446 AM3ST and AM3B. The total chemical production of glyoxal varies with the chemical
447 mechanisms, from 0.32 Tg/month with AM3B to 0.44 Tg/month with AM3ST. The
448 major sink of glyoxal with both mechanisms is photolysis, followed by aerosol uptake
449 and OH oxidation for AM3ST and OH oxidation and aerosol uptake for AM3B, although
450 the contribution of each pathway varies with mechanisms and γ_{glyx}. For example, in
451 AM3ST, heterogeneous loss is an important sink, accounting for 26% of the total
452 chemical loss of glyoxal; however, the contribution is negligible in the AM3B
453 simulations. Deposition accounts for only 1-2% of total glyoxal loss in the model. We

show in this work that the estimates of sources and sinks of glyoxal are dependent on the choice of gas-phase chemistry.

6 Conclusions and Discussion

A 0-D photochemical box model and a 3-D chemistry-climate model applied to data from the Southeast U.S. during the SENEX field campaign provide the first model evaluation of *in situ* glyoxal aircraft observations.

We find that the three mechanisms (AM3ST, AM3B, and MCM v3.3.1) show similarity in HCHO but large differences in glyoxal, leading to opposite NO_x dependence of R_{GF}. Under low NO_x conditions, the AM3 mechanisms predict much higher glyoxal yields than MCM v3.3.1, largely due to the significant contribution from isomerization of $ISOPO_2$ and oxidation of IEPOX via the $ISOPO_2$+HO_2 pathway. Although the three mechanisms agree better under high NO_x conditions, they show different pathways contributing to glyoxal production.

With the constraints from field measurements during SENEX, AM3ST with an effective reactive uptake coefficient γ_{glyx} of 2×10^{-3} and AM3B without heterogeneous loss of glyoxal can best reproduce the observed vertical profile. The latter shows better agreement with observed R_{GF} in the boundary layer. These two choices lead to less than 0.8 μg m^{-3} or negligible of glyoxal SOA in the boundary over the Southeast U.S., accounting for 0-14% of the total SOA in this region (Figure S7). These are likely the lower limit of glyoxal SOA due to missing sources of glyoxal that are not included in our model. Over North America, glyoxal sinks are dominated by photolysis, followed by

475 aerosol uptake and OH oxidation for AM3ST and OH oxidation and aerosol uptake for
476 AM3B. Dry and wet deposition are negligible for both AM3 versions (Table 1).

477 In the boundary layer, observations suggest a very similar NO_x dependence for
478 HCHO and glyoxal, resulting in a nearly constant R_{GF} across NO_x levels [*Kaiser et al.*,
479 2015]. Both AM3ST and AM3B can roughly capture the NO_x dependence of HCHO and
480 glyoxal, although AM3ST tends to overestimate R_{GF} at all NO_x regimes, likely due to the
481 overestimate of glyoxal at low NO_x and underestimate of HCHO across NO_x regimes.
482 AM3B shows a positive bias in R_{GF} at $NO_x < 0.5$ ppbv due to insufficient production of
483 HCHO. The MCM v3.3.1 like mechanism ("AM3M") shows a large underestimate of
484 glyoxal across all NO_x levels. One possible reason is the lack of a radical propagating
485 channel for the IEPOXOO + HO_2 reaction in MCM v3.3.1.

486 While glyoxal has been studied extensively over the past decade to understand the
487 magnitude of its heterogeneous uptake, we show here that its gas-phase production is a
488 large source of uncertainty that requires equal consideration. We find that its production
489 from isoprene oxidation varies greatly among different chemical mechanisms. This in
490 turn greatly impacts global estimates of glyoxal and in particular its contribution to SOA,
491 especially in regions with low to moderate NO_x levels (Figure 1). Under high NO_x
492 conditions, models differ significantly in the production of glyoxal from oxidation of
493 glycolaldehyde, as well as the fate of δ-$ISOPO_2$. Under low NO_x conditions, there is very
494 little laboratory evidence available on the production of glyoxal from IEPOX, HPALDs,
495 di-HPCARPs or other intermediate products. Although heterogeneous loss of IEPOX is
496 not included in current work, sensitivity tests show that inclusion of this uptake reduces
497 glyoxal concentrations by 10-20% for the mean vertical profile over the Southeast U.S.

Thus, the fate of IEPOX represents another mechanistic uncertainty for predicting glyoxal. Also, there are missing sources that are not represented in our model [*Volkamer et al.*, 2015] would increase modeled glyoxal and thus also inferred SOA. Future laboratory measurements are urgently needed and may have important implications for understanding the contribution of glyoxal to SOA in past and future atmospheres.

Acknowledgement

The authors thank Charles A. Brock (NOAA) for providing aerosol size data, Vaishali Naik (UCAR/NOAA) for providing emission inventories from the SENEX campaign, and William Cooke for the help with convection scheme of the AM3 model. JL, JM and LWH acknowledge supports by the NOAA Climate Program Office grant # NA13OAR4310071. KEM, RAW and SSB acknowledge support from the NOAA Atmospheric Chemistry, Climate and Carbon Cycle (AC4) program. JK, FNK, GMW, and TFH are grateful for support from EPA Science to Achieve Results (STAR) program grant 83540601 and NASA grant NNH10ZDA001N-SEAC4RS. J. Kaiser acknowledges support from NASA Headquarters under the NASA Earth and Space Science Fellowship Program – grant NNX14AK97H. RV is grateful for support from NSF EAGER award AGS-1452317. VFM acknowledges support from NSF (AGS-1546136). We thank the staff at the NOAA Aircraft Operations Center and the WP-3D flight crew for the help in instrumenting the aircraft and for conducting the flights. Special thanks go to Songmiao Fan (NOAA) for helpful discussions. This research has not been subjected to any EPA review and therefore does not necessarily reflect the views of the agency, and no official endorsement should be inferred. Observational data sets and modeling results are available upon request to the corresponding author (Jingqiu.Mao@noaa.gov).

References

Anderson, D. C., et al. (2014), Measured and modeled CO and NOy in DISCOVER-AQ: An evaluation of emissions and chemistry over the eastern US, *Atmos. Environ.*, *96*, 78-87, doi:http://dx.doi.org/10.1016/j.atmosenv.2014.07.004.

Bates, K. H., J. D. Crounse, J. M. St. Clair, N. B. Bennett, T. B. Nguyen, J. H. Seinfeld, B. M. Stoltz, and P. O. Wennberg (2014), Gas Phase Production and Loss of Isoprene Epoxydiols, *J. Phys. Chem. A*, *118*(7), 1237-1246, doi:10.1021/jp4107958.

Butkovskaya, N. I., N. Pouvesle, A. Kukui, and G. Le Bras (2006), Mechanism of the OH-Initiated Oxidation of Glycolaldehyde over the Temperature Range 233−296 K, *J. Phys. Chem. A*, *110*(50), 13492-13499, doi:10.1021/jp064993k.

Carlton, A. G., B. J. Turpin, K. E. Altieri, S. Seitzinger, A. Reff, H.-J. Lim, and B. Ervens (2007), Atmospheric oxalic acid and SOA production from glyoxal: Results of aqueous photooxidation experiments, *Atmos. Environ.*, *41*(35), 7588-7602, doi:http://dx.doi.org/10.1016/j.atmosenv.2007.05.035.

Cazorla, M., G. M. Wolfe, S. A. Bailey, A. K. Swanson, H. L. Arkinson, and T. F. Hanisco (2015), A new airborne laser-induced fluorescence instrument for in situ detection of formaldehyde throughout the troposphere and lower stratosphere, *Atmos. Meas. Tech.*, *8*(2), 541-552, doi:10.5194/amt-8-541-2015.

Corrigan, A. L., S. W. Hanley, and D. O. De Haan (2008), Uptake of Glyoxal by Organic and Inorganic Aerosol, *Environ. Sci. Technol.*, *42*(12), 4428-4433, doi:10.1021/es7032394.

543 Crounse, J. D., F. Paulot, H. G. Kjaergaard, and P. O. Wennberg (2011), Peroxy radical
544 isomerization in the oxidation of isoprene, *Phys. Chem. Chem. Phys.*, *13*(30), 13607-
545 13613, doi:10.1039/c1cp21330j.
546 DiGangi, J. P., et al. (2012), Observations of glyoxal and formaldehyde as metrics for the
547 anthropogenic impact on rural photochemistry, *Atmos. Chem. Phys.*, *12*(20), 9529-
548 9543, doi:10.5194/acp-12-9529-2012.
549 Dillon, T. J., and J. N. Crowley (2008), Direct detection of OH formation in the reactions
550 of HO2 with CH3C(O)O2 and other substituted peroxy radicals, *Atmos. Chem. Phys.*,
551 *8*(16), 4877-4889, doi:10.5194/acp-8-4877-2008.
552 Donner, L. J., et al. (2011), The Dynamical Core, Physical Parameterizations, and Basic
553 Simulation Characteristics of the Atmospheric Component AM3 of the GFDL Global
554 Coupled Model CM3, *J. Clim.*, *24*(13), 3484-3519, doi:10.1175/2011jcli3955.1.
555 Emmerson, K. M., and M. J. Evans (2009), Comparison of tropospheric gas-phase
556 chemistry schemes for use within global models, *Atmos. Chem. Phys.*, *9*(5), 1831-
557 1845, doi:10.5194/acp-9-1831-2009.
558 Ervens, B., B. J. Turpin, and R. J. Weber (2011), Secondary organic aerosol formation in
559 cloud droplets and aqueous particles (aqSOA): a review of laboratory, field and
560 model studies, *Atmos. Chem. Phys.*, *11*(21), 11069-11102, doi:10.5194/acp-11-
561 11069-2011.
562 Feierabend, K. J., J. E. Flad, S. S. Brown, and J. B. Burkholder (2009), HCO Quantum
563 Yields in the Photolysis of HC(O)C(O)H (Glyoxal) between 290 and 420 nm, *J. Phys.*
564 *Chem. A*, *113*(27), 7784-7794, doi:10.1021/jp9033003.

565 Fu, T.-M., D. J. Jacob, F. Wittrock, J. P. Burrows, M. Vrekoussis, and D. K. Henze
566 (2008), Global budgets of atmospheric glyoxal and methylglyoxal, and implications
567 for formation of secondary organic aerosols, *J. Geophys. Res. Atmos.*, *113*(D15),
568 D15303, doi:10.1029/2007jd009505.
569 Galloway, M. M., P. S. Chhabra, A. W. H. Chan, J. D. Surratt, R. C. Flagan, J. H.
570 Seinfeld, and F. N. Keutsch (2009), Glyoxal uptake on ammonium sulphate seed
571 aerosol: reaction products and reversibility of uptake under dark and irradiated
572 conditions, *Atmos. Chem. Phys.*, *9*(10), 3331-3345, doi:10.5194/acp-9-3331-2009.
573 Galloway, M. M., A. J. Huisman, L. D. Yee, A. W. H. Chan, C. L. Loza, J. H. Seinfeld,
574 and F. N. Keutsch (2011a), Yields of oxidized volatile organic compounds during the
575 OH radical initiated oxidation of isoprene, methyl vinyl ketone, and methacrolein
576 under high-NOx conditions, *Atmos. Chem. Phys.*, *11*(21), 10779-10790,
577 doi:10.5194/acp-11-10779-2011.
578 Galloway, M. M., C. L. Loza, P. S. Chhabra, A. W. H. Chan, L. D. Yee, J. H. Seinfeld,
579 and F. N. Keutsch (2011b), Analysis of photochemical and dark glyoxal uptake:
580 Implications for SOA formation, *Geophys. Res. Lett.*, *38*, L17811,
581 doi:10.1029/2011gl048514.
582 Gaston, C. J., T. P. Riedel, Z. Zhang, A. Gold, J. D. Surratt, and J. A. Thornton (2014),
583 Reactive Uptake of an Isoprene-Derived Epoxydiol to Submicron Aerosol Particles,
584 *Environ. Sci. Technol.*, *48*(19), 11178-11186, doi:10.1021/es5034266.
585 Gomez, M. E., Y. Lin, S. Guo, and R. Zhang (2015), Heterogeneous Chemistry of
586 Glyoxal on Acidic Solutions. An Oligomerization Pathway for Secondary Organic
587 Aerosol Formation, *J. Phys. Chem. A*, *119*(19), 4457-4463, doi:10.1021/jp509916r.

588 Guenther, A., T. Karl, P. Harley, C. Wiedinmyer, P. I. Palmer, and C. Geron (2006),
589 Estimates of global terrestrial isoprene emissions using MEGAN (Model of
590 Emissions of Gases and Aerosols from Nature), *Atmos. Chem. Phys.*, *6*(11), 3181-
591 3210, doi:10.5194/acp-6-3181-2006.
592 Hasson, A. S., G. S. Tyndall, and J. J. Orlando (2004), A Product Yield Study of the
593 Reaction of HO2 Radicals with Ethyl Peroxy (C2H5O2), Acetyl Peroxy
594 (CH3C(O)O2), and Acetonyl Peroxy (CH3C(O)CH2O2) Radicals, *J. Phys. Chem. A*,
595 *108*(28), 5979-5989, doi:10.1021/jp048873t.
596 Hastings, W. P., C. A. Koehler, E. L. Bailey, and D. O. De Haan (2005), Secondary
597 Organic Aerosol Formation by Glyoxal Hydration and Oligomer Formation:
598 Humidity Effects and Equilibrium Shifts during Analysis, *Environ. Sci. Technol.*,
599 *39*(22), 8728-8735, doi:10.1021/es050446l.
600 Hays, M. D., C. D. Geron, K. J. Linna, N. D. Smith, and J. J. Schauer (2002), Speciation
601 of Gas-Phase and Fine Particle Emissions from Burning of Foliar Fuels, *Environ. Sci.*
602 *Technol.*, *36*(11), 2281-2295, doi:10.1021/es0111683.
603 Hudman, R. C., et al. (2007), Surface and lightning sources of nitrogen oxides over the
604 United States: Magnitudes, chemical evolution, and outflow, *J. Geophys. Res. Atmos.*,
605 *112*(D12), doi:10.1029/2006JD007912.
606 Huijnen, V., J. E. Williams, and J. Flemming (2014), Modeling global impacts of
607 heterogeneous loss of HO2 on cloud droplets, ice particles and aerosols, *Atmos. Chem.*
608 *Phys. Discuss.*, *14*(6), 8575-8632, doi:10.5194/acpd-14-8575-2014.
609 Jacob, D. J. (2000), Heterogeneous chemistry and tropospheric ozone, *Atmos. Environ.*,
610 *34*(12–14), 2131-2159, doi:http://dx.doi.org/10.1016/S1352-2310(99)00462-8.

611 Jacobs, M. I., A. I. Darer, and M. J. Elrod (2013), Rate Constants and Products of the OH
612 Reaction with Isoprene-Derived Epoxides, *Environ. Sci. Technol.*, *47*(22), 12868-
613 12876, doi:10.1021/es403340g.
614 Jang, M., N. M. Czoschke, S. Lee, and R. M. Kamens (2002), Heterogeneous
615 Atmospheric Aerosol Production by Acid-Catalyzed Particle-Phase Reactions,
616 *Science*, *298*(5594), 814-817, doi:10.1126/science.1075798.
617 Jenkin, M. E., M. D. Hurley, and T. J. Wallington (2007), Investigation of the radical
618 product channel of the CH3C(O)O2 + HO2 reaction in the gas phase, *Phys. Chem.*
619 *Chem. Phys.*, *9*(24), 3149-3162, doi:10.1039/B702757E.
620 Jenkin, M. E., S. M. Saunders, and M. J. Pilling (1997), The tropospheric degradation of
621 volatile organic compounds: a protocol for mechanism development, *Atmos. Environ.*,
622 *31*(1), 81-104, doi:http://dx.doi.org/10.1016/S1352-2310(96)00105-7.
623 Jenkin, M. E., J. C. Young, and A. R. Rickard (2015), The MCM v3.3.1 degradation
624 scheme for isoprene, *Atmos. Chem. Phys.*, *15*(20), 11433-11459, doi:10.5194/acp-15-
625 11433-2015.
626 Kaiser, J., et al. (2015), Reassessing the ratio of glyoxal to formaldehyde as an indicator
627 of hydrocarbon precursor speciation, *Atmos. Chem. Phys.*, *15*(13), 7571-7583,
628 doi:10.5194/acp-15-7571-2015.
629 Kampf, C. J., E. M. Waxman, J. G. Slowik, J. Dommen, L. Pfaffenberger, A. P. Praplan,
630 A. S. H. Prévôt, U. Baltensperger, T. Hoffmann, and R. Volkamer (2013), Effective
631 Henry's Law Partitioning and the Salting Constant of Glyoxal in Aerosols Containing
632 Sulfate, *Environ. Sci. Technol.*, *47*(9), 4236-4244, doi:10.1021/es400083d.

633 Knote, C., et al. (2014), Simulation of semi-explicit mechanisms of SOA formation from
634 glyoxal in aerosol in a 3-D model, *Atmos. Chem. Phys.*, *14*(12), 6213-6239,
635 doi:10.5194/acp-14-6213-2014.
636 Kroll, J. H., N. L. Ng, S. M. Murphy, V. Varutbangkul, R. C. Flagan, and J. H. Seinfeld
637 (2005), Chamber studies of secondary organic aerosol growth by reactive uptake of
638 simple carbonyl compounds, *J. Geophys. Res. Atmos.*, *110*(D23207),
639 doi:10.1029/2005JD006004.
640 Kurtén, T., J. Elm, N. L. Prisle, K. V. Mikkelsen, C. J. Kampf, E. M. Waxman, and R.
641 Volkamer (2015), Computational Study of the Effect of Glyoxal–Sulfate Clustering
642 on the Henry's Law Coefficient of Glyoxal, *J. Phys. Chem. A*, *119*(19), 4509-4514,
643 doi:10.1021/jp510304c.
644 Lamarque, J. F., G. P. Kyle, M. Meinshausen, K. Riahi, S. Smith, D. van Vuuren, A.
645 Conley, and F. Vitt (2011), Global and regional evolution of short-lived radiatively-
646 active gases and aerosols in the Representative Concentration Pathways, *Clim.*
647 *Change*, *109*(1-2), 191-212, doi:10.1007/s10584-011-0155-0.
648 Lee, L., A. P. Teng, P. O. Wennberg, J. D. Crounse, and R. C. Cohen (2014), On Rates
649 and Mechanisms of OH and O3 Reactions with Isoprene-Derived Hydroxy Nitrates, *J.*
650 *Phys. Chem. A*, *118*(9), 1622-1637, doi:10.1021/jp4107603.
651 Li, J., M. Cleveland, L. D. Ziemba, R. J. Griffin, K. C. Barsanti, J. F. Pankow, and Q.
652 Ying (2015), Modeling regional secondary organic aerosol using the Master
653 Chemical Mechanism, *Atmos. Environ.*, *102*, 52-61,
654 doi:http://dx.doi.org/10.1016/j.atmosenv.2014.11.054.

655 Liggio, J., S.-M. Li, and R. McLaren (2005a), Heterogeneous Reactions of Glyoxal on
656 Particulate Matter: Identification of Acetals and Sulfate Esters, *Environ. Sci.*
657 *Technol.*, *39*(6), 1532-1541, doi:10.1021/es048375y.
658 Liggio, J., S.-M. Li, and R. McLaren (2005b), Reactive uptake of glyoxal by particulate
659 matter, *J. Geophys. Res. Atmos.*, *110*(D10), D10304, doi:10.1029/2004jd005113.
660 Lim, H.-J., A. G. Carlton, and B. J. Turpin (2005), Isoprene Forms Secondary Organic
661 Aerosol through Cloud Processing: Model Simulations, *Environ. Sci. Technol.*,
662 *39*(12), 4441-4446, doi:10.1021/es048039h.
663 Lin, M., et al. (2012), Transport of Asian ozone pollution into surface air over the
664 western United States in spring, *J. Geophys. Res. Atmos.*, *117*, D00V07,
665 doi:10.1029/2011jd016961.
666 Lockwood, A. L., P. B. Shepson, M. N. Fiddler, and M. Alaghmand (2010), Isoprene
667 nitrates: preparation, separation, identification, yields, and atmospheric chemistry,
668 *Atmos. Chem. Phys.*, *10*(13), 6169-6178, doi:10.5194/acp-10-6169-2010.
669 MacDonald, S. M., H. Oetjen, A. S. Mahajan, L. K. Whalley, P. M. Edwards, D. E.
670 Heard, C. E. Jones, and J. M. C. Plane (2012), DOAS measurements of formaldehyde
671 and glyoxal above a south-east Asian tropical rainforest, *Atmos. Chem. Phys.*, *12*(13),
672 5949-5962, doi:10.5194/acp-12-5949-2012.
673 Mao, J., L. W. Horowitz, V. Naik, S. Fan, J. Liu, and A. M. Fiore (2013a), Sensitivity of
674 tropospheric oxidants to biomass burning emissions: implications for radiative
675 forcing, *Geophys. Res. Lett.*, *40*(6), 1241-1246, doi:10.1002/grl.50210.

Mao, J., et al. (2010), Chemistry of hydrogen oxide radicals (HOx) in the Arctic troposphere in spring, *Atmos. Chem. Phys.*, *10*(13), 5823-5838, doi:10.5194/acp-10-5823-2010.

Mao, J., F. Paulot, D. J. Jacob, R. C. Cohen, J. D. Crounse, P. O. Wennberg, C. A. Keller, R. C. Hudman, M. P. Barkley, and L. W. Horowitz (2013b), Ozone and organic nitrates over the eastern United States: Sensitivity to isoprene chemistry, *J. Geophys. Res. Atmos.*, *118*(19), 11,256-211,268, doi:10.1002/jgrd.50817.

Marais, E. A., et al. (2016), Aqueous-phase mechanism for secondary organic aerosol formation from isoprene: application to the southeast United States and co-benefit of SO2 emission controls, *Atmos. Chem. Phys.*, *16*(3), 1603-1618, doi:10.5194/acp-16-1603-2016.

Miller, C. C., G. G. Abad, H. Wang, X. Liu, T. Kurosu, D. J. Jacob, and K. Chance (2014), Glyoxal retrieval from the Ozone Monitoring Instrument, *Atmos. Meas. Tech. Discuss.*, *7*(6), 6065-6112, doi:10.5194/amtd-7-6065-2014.

Millet, D. B., D. J. Jacob, K. F. Boersma, T.-M. Fu, T. P. Kurosu, K. Chance, C. L. Heald, and A. Guenther (2008), Spatial distribution of isoprene emissions from North America derived from formaldehyde column measurements by the OMI satellite sensor, *J. Geophys. Res. Atmos.*, *113*, D02307, doi:10.1029/2007jd008950.

Min, K. E., et al. (2015), A broadband cavity enhanced absorption spectrometer for aircraft measurements of glyoxal, methylglyoxal, nitrous acid, nitrogen dioxide, and water vapor, *Atmos. Meas. Tech. Discuss.*, *8*(10), 11209-11254, doi:10.5194/amtd-8-11209-2015.

698 Müller, J. F., J. Peeters, and T. Stavrakou (2014), Fast photolysis of carbonyl nitrates
699 from isoprene, *Atmos. Chem. Phys.*, *14*(5), 2497-2508, doi:10.5194/acp-14-2497-
700 2014.
701 Myriokefalitakis, S., M. Vrekoussis, K. Tsigaridis, F. Wittrock, A. Richter, C. Brühl, R.
702 Volkamer, J. P. Burrows, and M. Kanakidou (2008), The influence of natural and
703 anthropogenic secondary sources on the glyoxal global distribution, *Atmos. Chem.*
704 *Phys.*, *8*(16), 4965-4981, doi:10.5194/acp-8-4965-2008.
705 Naik, V., L. W. Horowitz, A. M. Fiore, P. Ginoux, J. Mao, A. M. Aghedo, and H. Levy
706 (2013), Impact of preindustrial to present-day changes in short-lived pollutant
707 emissions on atmospheric composition and climate forcing, *J. Geophys. Res. Atmos.*,
708 *118*(14), 8086-8110, doi:10.1002/jgrd.50608.
709 Nguyen, T. B., J. D. Crounse, A. P. Teng, J. M. St. Clair, F. Paulot, G. M. Wolfe, and P.
710 O. Wennberg (2015), Rapid deposition of oxidized biogenic compounds to a
711 temperate forest, *Proc. Natl. Acad. Sci*, *112*(5), E392-E401,
712 doi:10.1073/pnas.1418702112.
713 Niki, H., P. D. Maker, C. M. Savage, and M. D. Hurley (1987), Fourier transform
714 infrared study of the kinetics and mechanisms for the chlorine-atom- and hydroxyl-
715 radical-initiated oxidation of glycolaldehyde, *J. Phys. Chem*, *91*(8), 2174-2178,
716 doi:10.1021/j100292a038.
717 Nozière, B., P. Dziedzic, and A. Córdova (2009), Products and Kinetics of the Liquid-
718 Phase Reaction of Glyoxal Catalyzed by Ammonium Ions (NH4+), *J. Phys. Chem. A*,
719 *113*(1), 231-237, doi:10.1021/jp8078293.

720 Palmer, P. I., D. J. Jacob, A. M. Fiore, R. V. Martin, K. Chance, and T. P. Kurosu (2003),
721 Mapping isoprene emissions over North America using formaldehyde column
722 observations from space, *J. Geophys. Res. Atmos.*, *108*(D6), 4180,
723 doi:10.1029/2002JD002153.
724 Paulot, F., J. D. Crounse, H. G. Kjaergaard, J. H. Kroll, J. H. Seinfeld, and P. O.
725 Wennberg (2009a), Isoprene photooxidation: new insights into the production of
726 acids and organic nitrates, *Atmos. Chem. Phys.*, *9*(4), 1479-1501, doi:10.5194/acp-9-
727 1479-2009.
728 Paulot, F., J. D. Crounse, H. G. Kjaergaard, A. Kürten, J. M. St. Clair, J. H. Seinfeld, and
729 P. O. Wennberg (2009b), Unexpected Epoxide Formation in the Gas-Phase
730 Photooxidation of Isoprene, *Science*, *325*(5941), 730-733,
731 doi:10.1126/science.1172910.
732 Paulot, F., P. Ginoux, W. F. Cooke, L. J. Donner, S. Fan, M. Lin, J. Mao, V. Naik, and L.
733 W. Horowitz (2015), Sensitivity of nitrate aerosols to ammonia emissions and to
734 nitrate chemistry: implications for present and future nitrate optical depth, *Atmos.*
735 *Chem. Phys. Discuss.*, *15*(18), 25739-25788, doi:10.5194/acpd-15-25739-2015.
736 Peeters, J., J.-F. Müller, T. Stavrakou, and V. S. Nguyen (2014), Hydroxyl Radical
737 Recycling in Isoprene Oxidation Driven by Hydrogen Bonding and Hydrogen
738 Tunneling: The Upgraded LIM1 Mechanism, *J. Phys. Chem. A*, *118*(38), 8625-8643,
739 doi:10.1021/jp5033146.
740 Peeters, J., and T. L. Nguyen (2012), Unusually Fast 1,6-H Shifts of Enolic Hydrogens in
741 Peroxy Radicals: Formation of the First-Generation C2 and C3 Carbonyls in the
742 Oxidation of Isoprene, *J. Phys. Chem. A*, *116*(24), 6134-6141, doi:10.1021/jp211447q.

743 Praske, E., J. D. Crounse, K. H. Bates, T. Kurtén, H. G. Kjaergaard, and P. O. Wennberg
744 (2015), Atmospheric Fate of Methyl Vinyl Ketone: Peroxy Radical Reactions with
745 NO and HO2, *J. Phys. Chem. A, 119*(19), 4562-4572, doi:10.1021/jp5107058.
746 Pye, H. O. T., et al. (2013), Epoxide Pathways Improve Model Predictions of Isoprene
747 Markers and Reveal Key Role of Acidity in Aerosol Formation, *Environ. Sci.*
748 *Technol.*, *47*(19), 11056-11064, doi:10.1021/es402106h.
749 Rivera-Rios, J. C., et al. (2014), Conversion of hydroperoxides to carbonyls in field and
750 laboratory instrumentation: Observational bias in diagnosing pristine versus
751 anthropogenically controlled atmospheric chemistry, *Geophys. Res. Lett.*, *41*(23),
752 8645-8651, doi:10.1002/2014GL061919.
753 Sander, R. (2015), Compilation of Henry's law constants (version 4.0) for water as
754 solvent, *Atmos. Chem. Phys.*, *15*(8), 4399-4981, doi:10.5194/acp-15-4399-2015.
755 Saunders, S. M., M. E. Jenkin, R. G. Derwent, and M. J. Pilling (2003), Protocol for the
756 development of the Master Chemical Mechanism, MCM v3 (Part A): tropospheric
757 degradation of non-aromatic volatile organic compounds, *Atmos. Chem. Phys.*, *3*(1),
758 161-180, doi:10.5194/acp-3-161-2003.
759 St. Clair, J. M., J. C. Rivera-Rios, J. D. Crounse, H. C. Knap, K. H. Bates, A. P. Teng, S.
760 Jørgensen, H. G. Kjaergaard, F. N. Keutsch, and P. O. Wennberg (2016a), Kinetics
761 and Products of the Reaction of the First-Generation Isoprene Hydroxy
762 Hydroperoxide (ISOPOOH) with OH, *J. Phys. Chem. A, 120*(9), 1441-1451,
763 doi:10.1021/acs.jpca.5b06532.
764 St. Clair, J. M., J. C. Rivera-Rios, J. D. Crounse, E. Praske, M. J. Kim, G. M. Wolfe, F. N.
765 Keutsch, P. O. Wennberg, and T. F. Hanisco (2016b), Investigation of a potential

766 HCHO measurement artifact from ISOPOOH, *Atmos. Meas. Tech. Discuss.*, *2016*, 1-
767 15, doi:10.5194/amt-2016-204.
768 Stavrakou, T., J. F. Müller, I. De Smedt, M. Van Roozendael, M. Kanakidou, M.
769 Vrekoussis, F. Wittrock, A. Richter, and J. P. Burrows (2009), The continental source
770 of glyoxal estimated by the synergistic use of spaceborne measurements and inverse
771 modelling, *Atmos. Chem. Phys.*, *9*(21), 8431-8446, doi:10.5194/acp-9-8431-2009.
772 Stavrakou, T., J. Peeters, and J. F. Müller (2010), Improved global modelling of HOx
773 recycling in isoprene oxidation: evaluation against the GABRIEL and INTEX-A
774 aircraft campaign measurements, *Atmos. Chem. Phys.*, *10*(20), 9863-9878,
775 doi:10.5194/acp-10-9863-2010.
776 Teng, A. P., J. D. Crounse, L. Lee, J. M. St. Clair, R. C. Cohen, and P. O. Wennberg
777 (2015), Hydroxy nitrate production in the OH-initiated oxidation of alkenes, *Atmos.*
778 *Chem. Phys.*, *15*(8), 4297-4316, doi:10.5194/acp-15-4297-2015.
779 Travis, K., et al. (2015), Declining NO_x in the Southeast US and implications for ozone-
780 NO_x-VOC chemistry, in *SEAC^{4}RS Science Team Meeting*, edited, Pasadena,
781 California
782 Volkamer, R., et al. (2015), Aircraft measurements of BrO, IO, glyoxal, NO2, H2O, O2–
783 O2 and aerosol extinction profiles in the tropics: comparison with aircraft-/ship-based
784 in situ and lidar measurements, *Atmos. Meas. Tech.*, *8*(5), 2121-2148,
785 doi:10.5194/amt-8-2121-2015.
786 Volkamer, R., I. Barnes, U. Platt, L. T. Molina, and M. J. Molina (2006), Remote Sensing
787 of Glyoxal by Differential Optical Absorption Spectroscopy (DOAS): Advancements
788 in Simulation Chamber and Field Experiments, in *Environmental Simulation*

Chambers: Application to Atmospheric Chemical Processes, edited by I. Barnes and K. Rudzinski, pp. 129-141, Springer Netherlands, doi:10.1007/1-4020-4232-9_10.

Volkamer, R., L. T. Molina, M. J. Molina, T. Shirley, and W. H. Brune (2005), DOAS measurement of glyoxal as an indicator for fast VOC chemistry in urban air, *Geophys. Res. Lett.*, *32*, L08806, doi:10.1029/2005gl022616.

Volkamer, R., F. San Martini, L. T. Molina, D. Salcedo, J. L. Jimenez, and M. J. Molina (2007), A missing sink for gas-phase glyoxal in Mexico City: Formation of secondary organic aerosol, *Geophys. Res. Lett.*, *34*, L19807, doi:10.1029/2007gl030752.

Volkamer, R., P. J. Ziemann, and M. J. Molina (2009), Secondary Organic Aerosol Formation from Acetylene (C2H2): seed effect on SOA yields due to organic photochemistry in the aerosol aqueous phase, *Atmos. Chem. Phys.*, *9*(6), 1907-1928, doi:10.5194/acp-9-1907-2009.

Vrekoussis, M., F. Wittrock, A. Richter, and J. P. Burrows (2010), GOME-2 observations of oxygenated VOCs: what can we learn from the ratio glyoxal to formaldehyde on a global scale?, *Atmos. Chem. Phys.*, *10*(21), 10145-10160, doi:10.5194/acp-10-10145-2010.

Warneke, C., et al. (2010), Biogenic emission measurement and inventories determination of biogenic emissions in the eastern United States and Texas and comparison with biogenic emission inventories, *J. Geophys. Res. Atmos.*, *115*(D7), D00F18, doi:10.1029/2009jd012445.

Warneke, C., et al. (2016), Instrumentation and Measurement Strategy for the NOAA SENEX Aircraft Campaign as Part of the Southeast Atmosphere Study 2013, *Atmos. Meas. Tech. Discuss.*, *2016*, 1-39, doi:10.5194/amt-2015-388.

812 Washenfelder, R. A., et al. (2011), The glyoxal budget and its contribution to organic
813 aerosol for Los Angeles, California, during CalNex 2010, *J. Geophys. Res. Atmos.*,
814 *116*(D21), D00V02, doi:10.1029/2011jd016314.
815 Waxman, E. M., J. Elm, T. Kurtén, K. V. Mikkelsen, P. J. Ziemann, and R. Volkamer
816 (2015), Glyoxal and Methylglyoxal Setschenow Salting Constants in Sulfate, Nitrate,
817 and Chloride Solutions: Measurements and Gibbs Energies, *Environ. Sci. Technol.*,
818 *49*(19), 11500-11508, doi:10.1021/acs.est.5b02782.
819 Wolfe, G. M., et al. (2016), Formaldehyde production from isoprene oxidation
820 across NOx regimes, *Atmos. Chem. Phys.*, *16*(4), 2597-2610, doi:10.5194/acp-16-
821 2597-2016.
822 Xiong, F., et al. (2015), Observation of isoprene hydroxynitrates in the Southeastern
823 United States and implications for the fate of NOx, *Atmos. Chem. Phys. Discuss.*,
824 *15*(13), 17843-17886, doi:10.5194/acpd-15-17843-2015.
825 Ying, Q., J. Li, and S. H. Kota (2015), Significant Contributions of Isoprene to
826 Summertime Secondary Organic Aerosol in Eastern United States, *Environ. Sci.*
827 *Technol.*, *49*(13), 7834-7842, doi:10.1021/acs.est.5b02514.
828 Zhao, J., N. P. Levitt, R. Zhang, and J. Chen (2006), Heterogeneous Reactions of
829 Methylglyoxal in Acidic Media: Implications for Secondary Organic Aerosol
830 Formation, *Environ. Sci. Technol.*, *40*(24), 7682-7687, doi:10.1021/es060610k.

831

Table 1. Budget of glyoxal over North America (20 ~55 ºN, 60 ~130 ºW) below 1.5 km in June-July of 2013. Percentage is the contribution of each pathway to the total chemical loss of glyoxal.

	AM3ST	AM3B
γ_{glyx} ($\times 10^{-3}$)	2.0	0
Production (Tg/month)	**0.44**	**0.32**
Chemical Loss (Tg/month)	**0.41**	**0.29**
Photolysis	57%	77%
OH	17%	23%
Uptake by Aerosols	26%	–
Dry Deposition (Tg/month)	**1.2×10^{-2}**	**1.2×10^{-2}**
Wet Deposition (Tg/month)	**1.1×10^{-2}**	**1.6×10^{-2}**

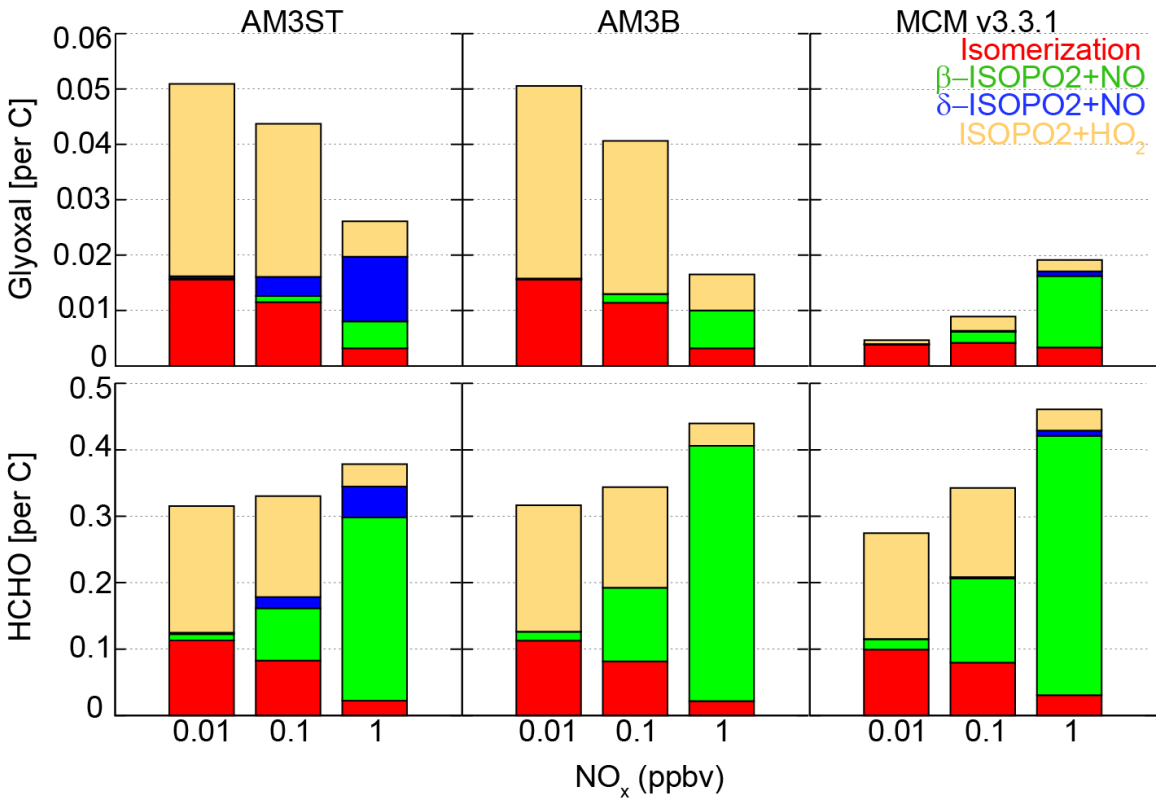

836

837 **Figure 1**. Cumulative yields of glyoxal and HCHO in major pathways from isoprene
838 oxidation at different NO_x levels. Glyoxal and HCHO from isoprene oxidized by O_3 and
839 by NO_3 are not shown due to low production in all the mechanisms.

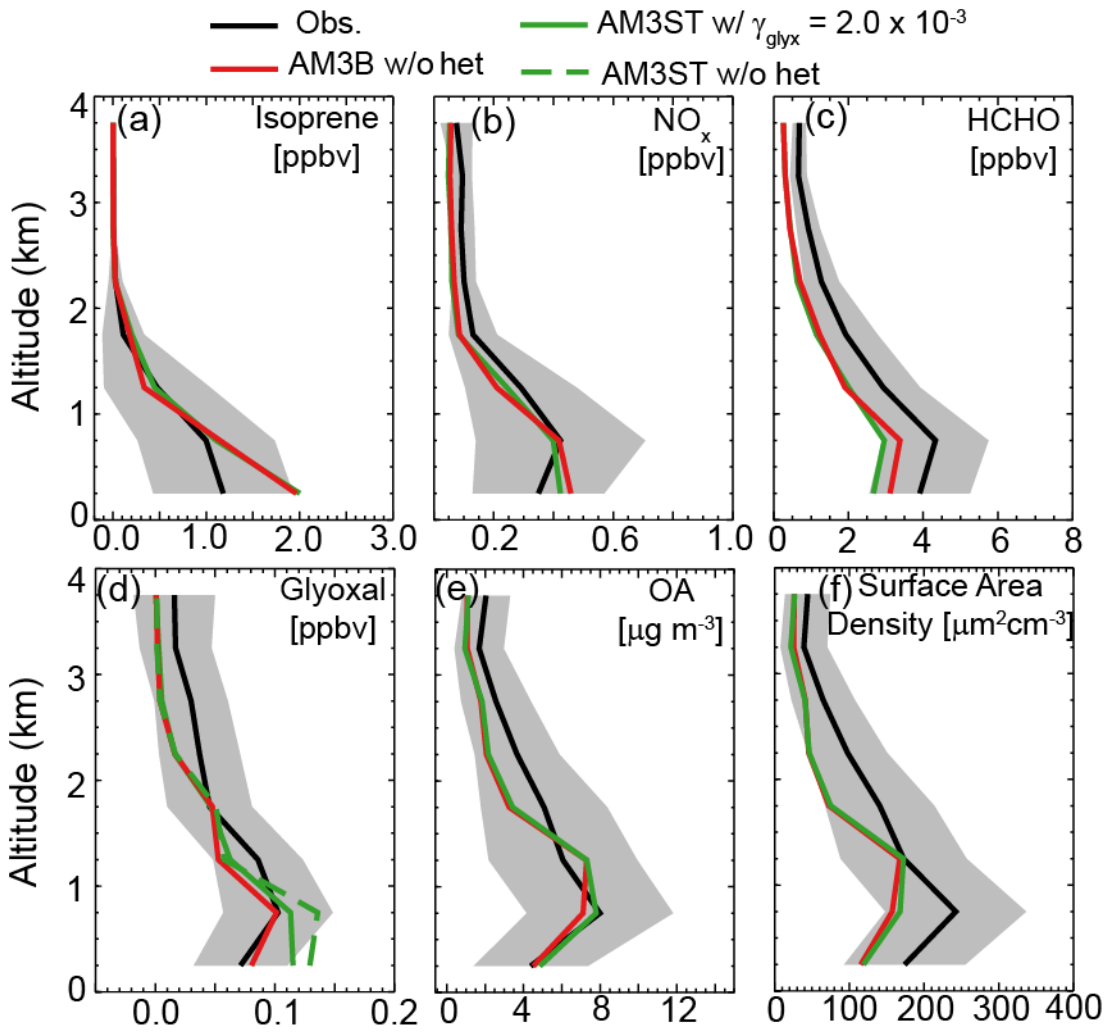

Figure 2. Mean vertical profiles of isoprene, formaldehyde, NO_x, glyoxal, organic aerosol (OA) and surface area density of aerosol during SENEX. Grey shades are the standard deviation (σ) of the averaged profiles of the measured tracers. Dashed green line in panel (d) is model estimate without heterogeneous loss of glyoxal by AM3ST. Observed organic aerosol mass and aerosol surface area density are from dry particles.

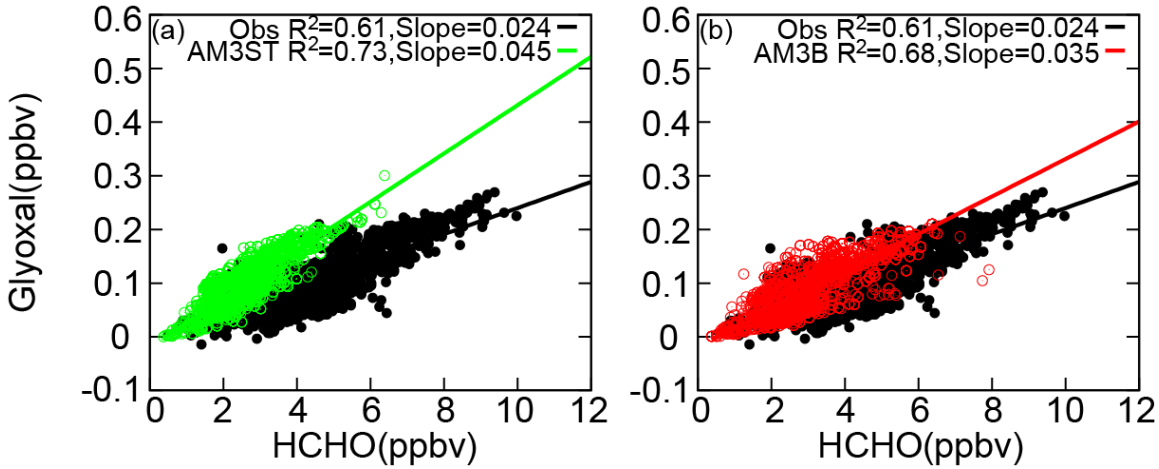

Figure 3. Correlation between glyoxal and formaldehyde below 1.5 km during SENEX. Black dots represent observations, while green and red open circles show AM3ST with $\gamma_{glyx} = 2.0 \times 10^{-3}$ (left) and AM3B without heterogeneous loss of glyoxal (right). Solid lines are linear regression lines, with regression slopes calculated from least-squares fit.

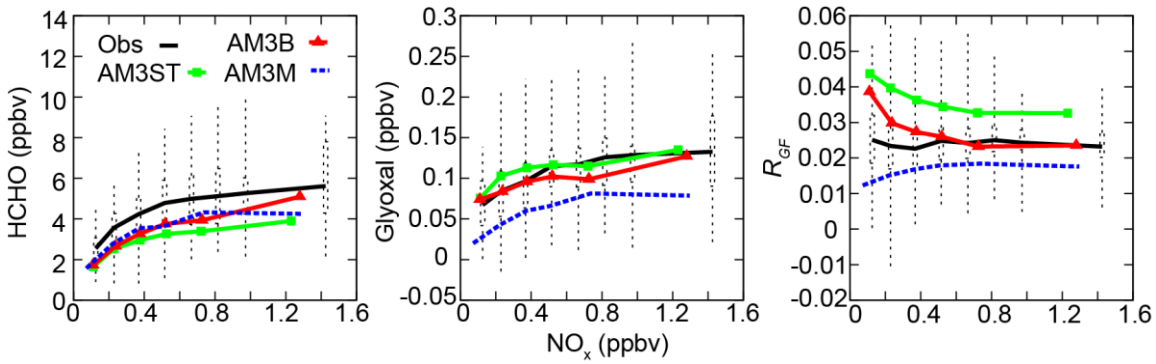

Figure 4. HCHO (ppbv), glyoxal (ppbv), and R_{GF} in each NO_x bin below 1.5 km during SENEX. Dots, dashed boxes and whiskers are the mean, interquartile range and lowest and highest of the observations; green squares and red triangles are the mean of AM3ST with $\gamma_{glyx}=2.0 \times 10^{-3}$ and AM3B without heterogeneous loss of glyoxal respectively; blue dashed lines are the mean of AM3M without heterogeneous loss of glyoxal.